

An anticancer drug to probe non-specific protein-DNA interactions

Abhigyan Sengupta, Rajkumar Koninti, Krishna Gavvala, Nirmalya Ballav, Partha Hazra*^a

^a *Department of Chemistry, Indian Institute of Science Education and Research (IISER), Pune
411021, Maharashtra, India.*

E-mail: p.hazra@iiserpune.ac.in.

Tel.: +91-20-2590-8077

Fax: +91-20-2589 9790.

Note 1: Experimental Section

(a) *Materials and methods*

Ellipticine (purity $\geq 99\%$), Bovine serum albumin (BSA, biochemistry grade), Human serum albumin (HSA, biochemistry grade), Calf Thymus DNA Na Salt (approximately 1000 bp long) and salmon sperm DNA (approximately 2000 bp long) were purchased from Sigma Aldrich and used without further purification. Molecular biology grade Na_2HPO_4 and NaH_2PO_4 are procured from Sisco Research Laboratories (SRL-India), whereas NaCl (BioXtra purity $\geq 99.5\%$), KCl (purity $\geq 99\%$) and EDTA (BioUltra purity $\geq 99\%$) were purchased from Sigma Aldrich. Phosphate buffer ($\text{Na}_2\text{HPO}_4 + \text{NaH}_2\text{PO}_4$, 10 mM) saline (PBS) of pH 7.2 (containing 137 mM NaCl, 3 mM KCl and 0.1 mM EDTA) was used for all experiments. All samples and buffer preparation were done in sterilized mili-Q water ($18.2 \mu\Omega \text{ cm}^{-1}$). The concentration of DNA stock solution was determined by using molar extinction coefficient $6600 \text{ M}^{-1} \cdot \text{cm}^{-1}/\text{base}$ for DNA at 260 nm. The individual solutions with different concentration were prepared by adding respective amount from stock. Serum proteins were quantified using its respective molar extinction coefficient at 280 nm, $43,824 \text{ M}^{-1} \text{ cm}^{-1}$ for BSA and $36500 \text{ M}^{-1} \text{ cm}^{-1}$ for HSA.

As ellipticine is sparingly soluble in water, we have used DMSO stock solution of ellipticine for all experiments. A 2 μL stock of ellipticine in DMSO was dissolved in 2.5 ml of PBS, and then the solution was strongly sonicated for ~ 1 hr (avoiding heating effect) to obtain a homogeneous ellipticine solution in water. This solution of ellipticine found to be stable enough for long duration even for few days, without any separation or precipitation of ellipticine from PBS. The working concentration of ellipticine was kept 10 μM for all the studies.

For steady state fluorescence measurements, a fixed concentration of ellipticine (10 μM) in PBS is first titrated with increasing concentrations of serum protein and then with DNA. In all cases sample containing ellipticine were excited at 350 nm and fluorescence emission was collected from 375 nm to 690 nm.

Field emission scanning electron microscopy experiments were done in same Phosphate buffer ($\text{Na}_2\text{HPO}_4 + \text{NaH}_2\text{PO}_4$, 10 mM) saline (PBS) of pH 7.2 (containing 137 mM NaCl, 3 mM

KCl and 0.1 mM EDTA). Respective concentration of protein and DNA had been maintained in PBS, drop-casted in a silicon wafer and dried in vacuum overnight.

Instrumentations

Measurements of solution pH were done by pH-1500 (Eutech Instruments, USA) and cross verified by silicon micro sensor pocket sized pH meter (ISFETCOM. Co. Ltd., Japan). Absorption spectra of free and protein/DNA bound ellipticine were recorded in Evolution-300 UV-Visible spectrophotometer (Thermo Fisher Scientific, USA). Steady state fluorescence measurements were executed in Fluorolog-3 (Horiba Jobin Yvon, USA) where the samples are excited at 350 nm and the collection range has been arranged accordingly.

Fluorescence lifetime and time resolved anisotropy measurements were performed using time-correlated single photon counting (TCSPC) set-up from IBH Horiba Jobin Yvon (USA). Detail description of the instrument is mentioned elsewhere.¹⁻⁴ The lifetime and anisotropy data were collected at the respective peak maximum of sample using 375 nano-LED (FWHM=90 ps) for excitation. We have used IBH DAS6 software for the analysis of data. Quality of lifetime and anisotropy fits was judged on basis χ^2 values and the visual inspection of the residuals. The value of $\chi^2 \approx 1$ was considered as best fit for the plots.

Circular dichroism (CD) spectra were recorded on a J-815 CD (JASCO, USA). Each CD profile is an average of 5 scans of the same sample collected at a scan speed 20 nm/min, with a proper baseline correction of the blank buffer. During CD measurement, BSA concentration was kept fixed and the concentrations of ellipticine were increased steadily.

The field emission scanning electron microscope (FE-SEM) images of blank serum albumin, CT-DNA and protein-DNA assemble were collected by ZEISS, Ultra Plus.

(b) Molecular docking

The crystal structure of protein was taken from RSCB protein Data Bank (PDB)⁵ having a PDB ID:3V03. A dimeric BSA crystal structure was obtained with associated crystalline water molecules and calcium ions. One of the monomeric units of BSA, water molecules and calcium ions were removed from the crystal structure. The energy optimization of ellipticine conformers have been done using HF/6-31G level of Gaussian 98 suite and the resultant energy minimized geometry was saved in Autodock 4.2^{6, 7} compatible format. We have used Lamarckian Generic Algorithm^{6, 7} to find out the binding locations of ellipticine in BSA in Autodock 4.2 software. At the beginning of the study all water molecules was removed and Gasteiger charges were computed followed by addition of hydrogen as required by Lamarckian Generic Algorithm.^{7, 8} At the initial stage as the approximate location of binding was not known, we fixed a $126 \times 126 \times 126$ grid box dimensions along x, y, and z axes with grid spacing 0.56 Å to cover all the atoms of BSA, and a blind docking was performed to locate the possible position of the probe in BSA. Ellipticine was docked in BSA with 150 GA population size and 100 GA runs. The lowest possible energy structure has been searched out using rank by energy presentation. After respective three repetitions, the minimum energy structure was taken for further analysis. After selecting the possible locations of ellipticine, the size of grid box was decreased to $60 \times 60 \times 60$ in respective directions with a grid spacing 0.375 Å to generate most stable docked form through finite docking studies. The respective structure has been used for visualization through python molecular viewer.^{6, 7} The final structure for presentation has been generated using chimera.⁹

Note 2: Protein -Ellipticine Interaction

(a) Steady State Results

Ellipticine in phosphate buffer saline of physiological pH (**Note 1**) exhibits a single, broad and unstructured emission at 525 nm (**Figure S1**), which is attributed to protonated ellipticine where quinoline nitrogen gets protonated as its intrinsic protonation pK_a in water is 7.4.¹⁰ A dramatic modification of ellipticine emission has been observed with increasing concentration of serum albumin (BSA & HSA) (**Figure S1**). At very first addition of serum albumin (SA) (0.25 μ M), a new peak starts appearing around 440 nm, strongly rises with upraising SA concentrations, and finally gets saturated at higher protein additions (maximum 110 μ M). It is already reported that when ellipticine resides in hydrophobic environment, apparent pK_a of quinoline nitrogen drops down to ~ 6 due to reduced polarity,¹⁰ which facilitates the transformation from protonated to neutral form of ellipticine.^{10, 11} Moreover, in low dielectric solvents, ellipticine exhibits high energy emission peak mainly originated from neutral form.¹¹⁻¹³ Therefore, the emission peak at 440 nm is ascribed to the neutral ellipticine molecules bound to serum albumin (BSA/HSA), which is in close agreement with recent results reported at low protein concentration¹⁴. Relative comparison with previous results shows ellipticine exhibits a peak at ~ 444 nm in methanol and ethanol having $E_T(30)$ value of 55.4 and 51.90,¹⁵ respectively. Hence, neutral ellipticine experiences a polarity value close to ~ 53.5 in $E_T(30)$ scale inside the protein binding pocket. Ellipticine constituted by extended aromatic rings is highly hydrophobic and the hydrophobic-hydrophobic interaction between protein and drug drags the molecule inside protein pocket away from high polarity milieu of water (63.1 in $E_T(30)$ scale). With every addition of SA more hydrophobic vicinity has been created around the drug molecules, which modulates the emission behaviour of ellipticine, and plays a crucial role for the fluorescence switching from 525 nm to 440 nm. Unlike 440 nm, emission at 525 nm does not shoot up drastically but an apparent enhancement of fluorescence intensity is observed with increasing SA concentrations (**Figure S1**). Deconvoluted spectra show prominent intensity rise at 525 nm along with a dominant blue shift (**Figure S1**), which infers that a fraction of protonated ellipticine molecules are also moving inside binding pocket of serum proteins. The reduced polarity at binding pockets might be responsible for the blue shift of the protonated peak.

A quantitative estimation of drug-protein interaction is always important since the interaction

efficiency and influence of the drug on protein structure governs the therapeutic importance of the drug.^{16, 17} Ellipticine-BSA binding constant was elucidated using modified Scatchard plot^{18, 19} (Note 2c, Figure S3) which offers $K = (2.75 \pm 0.138) \times 10^5 \text{ M}^{-1}$ for 440 nm emission. The binding constant along with high free energy change ($\Delta G^0 = -7.41 \text{ kcal.mol}^{-1}$ at 298 K) implies that the binding interaction between neutral ellipticine and BSA is energetically favoured. The binding constant measured at 525 nm ($(2.50 \pm 0.126) \times 10^5 \text{ M}^{-1}$) and free energy change ($-7.30 \text{ kcal.mol}^{-1}$) for the complexation, clearly implies that the protonated ellipticine also has strong affinity towards BSA and definitely is also an energy favoured process. Values determined for K and ΔG^0 are found to be in good accordance with literature reports for several other probe-protein interaction studies.^{2, 20-23} The steady state anisotropy results collected at 440 nm and 525 nm emissions also conclude an effective binding interaction between both the forms (neutral and protonated) of the drug and protein (Note 2d, Figure S4). We anticipate that domain I characterized by net negative charge^{24, 25} can serve as a suitable binding site for protonated ellipticine (as it contains one unit positive charge), whereas domain II or III, being dominantly hydrophobic^{24, 25} is the most probable location for neutral ellipticine.

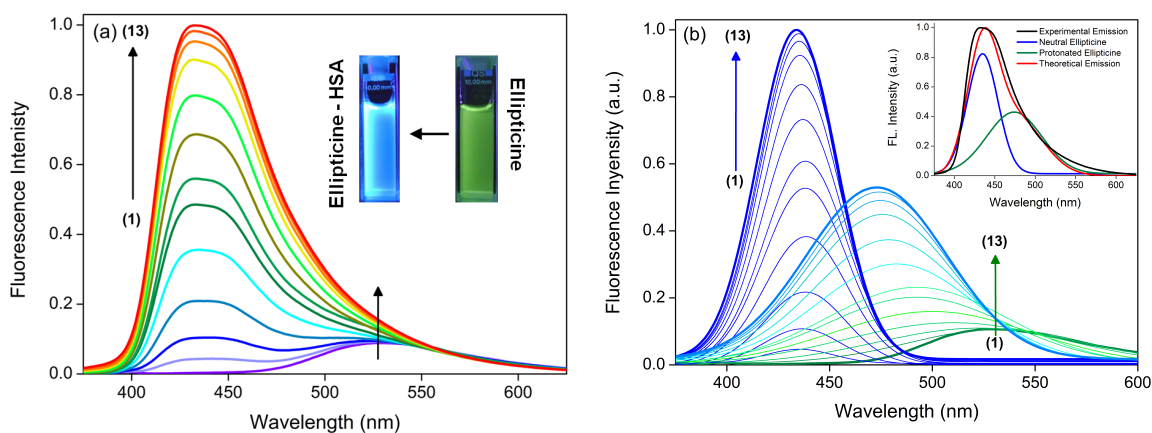


Figure S1: (c) Fluorescence emission intensity of ellipticine with variable HSA {[HSA] = 0, 0.25, 0.50, 1, 3, 6, 10, 20, 30, 50, 70, 90 and 110 μM respectively (1→13)}. Inset shows the color switch by HSA addition. (d) Deconvoluted emission intensity of ellipticine with variable HSA concentrations, where inset stand for a sample deconvolution.

The steady state results validated well from time resolved measurements where we found a steady increase in lifetime values of 440 nm (neutral ellipticine) as well as 525 nm (protonated conformer) collections (Note 2e). Moreover the trends in time resolved anisotropy (Note 2f) establishes the basis of our claim and discussed thoroughly in supporting information. To extend

the applicability of our work we have also monitored interaction of ellipticine with human serum albumin (BSA) under similar experimental conditions.

(b) Molecular Modelling

An understanding about the location of drug in protein cavity is always important in order to judge the carriage and therapeutic efficiency of the drug. To obtain a notion about the binding sites we choose energy minimized structures (using Gaussian 98) of the neutral as well as protonated forms of ellipticine (**Scheme 1**). The most probable binding site for protonated ellipticine is found to be domain IB (**Figure S2**), whereas lowest energy binding site for neutral ellipticine is determined to be domain III A (**Figure 1, main manuscript**). Protonated ellipticine in domain IB is surrounded by ASP107, ASP108, SER109, PRO110, ARG144, HIS145, PRO146, TYR147, SER191, SER192, ALA193, ARG196 and ARG458 amino acids, and feels a strong electrostatic drag towards this domain.^{20, 26-28} Moreover, protonated ellipticine involves in hydrogen bonding interaction with HIS145 (**Figure S2**), and contributes towards the net favourable binding free energy of -9.03 kcal/mol. The docking study also reveals that neutral form of the drug in domain IIIA is surrounded by the amino acids GLU382, PRO383, LEU386, ILE387, ASN390, CYS391, PHE402, LEU406, ASG409, LEU429, ALA432, GLY433, CYS437, MET445, THR448, GLU449, LEU452 and ARG484, and provides a binding free energy change of -7.8 kcal/mol. In summary, the docking results validate well the experimental observations, where we have found enough evidence for the binding of both the forms of ellipticine with serum albumin.

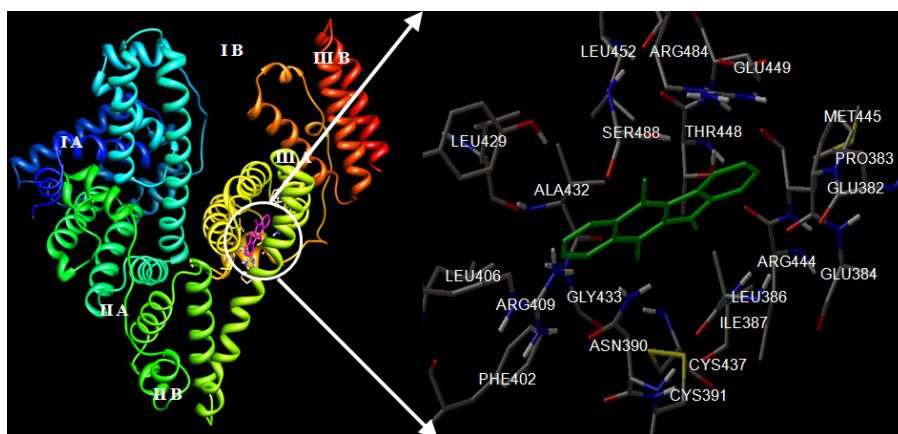


Figure S2: Docked conformation of ellipticine with BSA. Protonated ellipticine bound to domain IB, where inset shows the magnified view of binding site along with hydrogen bonding interaction.

(c) Binding constant determination from steady state emission results using modified Scatchard Plot

Ellipticine-BSA binding has been elucidated using modified Scatchard plot^{18, 19} which is described as follows

$$\frac{[M]_{\text{total}}}{f} = \frac{1}{NK_f(1-f)} + \frac{[L]_{\text{total}}}{N} \quad (1)$$

Where, $[M]_{\text{total}}$ is the final concentration of the protein, $[L]_{\text{total}}$ is the total concentration of the drug, “N” is the number of sites in protein and “f” represents the fraction of ligand bound to macromolecule. The value of “f” can be evaluated from the following equation

$$f = \frac{(I_{\text{obs}} - I_L)}{(I_{\text{max}} - I_L)} \quad (2)$$

Where I_{obs} , I_L , and I_{max} represents observed fluorescence from each addition, intensity of the free drug and maximum intensity after saturation of all binding sites, respectively. A plot of $[M]_{\text{total}}/f$ vs. $1/(1-f)$ produces a straight line and one can calculate association constant (K_f) for protein-drug interaction from the slope (**Figure S3**).

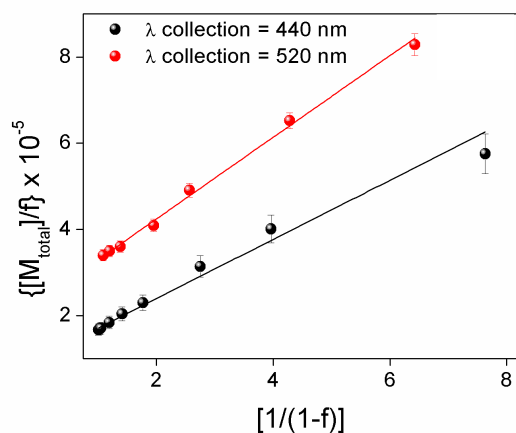


Figure S3: Ellipticine-BSA modified Scatchard plot, where legends carry the respective meanings.

(d) Steady state anisotropy results

Anisotropy measurement can offer a vivid perception about the bound and an unbound state of the molecule,²⁹ hence, this technique is employed to explore ellipticine and BSA binding interaction. The difference of anisotropy between free and bound drug molecules can be utilized extensively to evaluate the location of the probe in macro structures.^{2, 20, 30} When drug molecules reside in protein binding pocket, the rotational motion of the drug retards severely, and it leads to the high anisotropy value of the drug. **Figure S4** depicts the change of steady state anisotropy for both neutral and protonated ellipticine with the increasing concentrations of protein. In both the cases, a steep rise followed by saturation in anisotropy value is observed (**Figure S4**). The steep rise in the anisotropy indicates increasing restriction of rotational motion of drug, and the attainment of plateau implies the saturation in the binding interaction between the drug and protein.

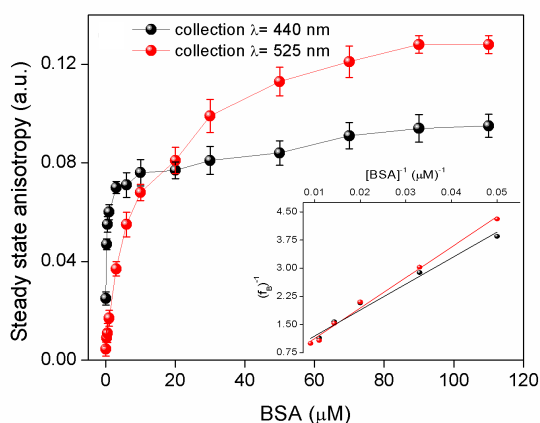


Figure S4: Steady state anisotropy of ellipticine with increasing BSA concentration, inset shows the binding curve generated from anisotropy data.

The applicability of anisotropy measurements has been extended by determining the association constant for drug-protein interaction. Binding constant (K_f) is determined using the following equations²⁹

$$\frac{1}{f_B} = 1 + \frac{1}{K_f[\text{protein}]} \quad (3)$$

$$f_B = \frac{(r - r_F)}{R(r_B - r) + (r - r_F)} \quad (4)$$

Where, f_B is fraction of drug molecules bound to protein, and r_F , r_B are the anisotropy of free and bound drug, respectively. R is the correction factor (ratio of bound/free drug intensities measured under same experimental conditions). The binding constant is determined from the slope from the plot $1/f_B$ vs $1/[\text{protein}]$ (**inset of Figure S4**). The binding constants evaluated for neutral and protonated ellipticine are $1.27 \times 10^5 \text{ M}^{-1}$ and $1.15 \times 10^5 \text{ M}^{-1}$ respectively, are in close agreement with steady state emission measurements. Therefore, anisotropy data also supports our steady state emission results where we have seen that both protonated and neutral ellipticine molecules strongly interact with protein.

(e) Time resolved lifetime results:

Fluorescence lifetime measurement is an excellent technique to explore the excited state environment around the fluorophore and is highly sensitive to the excited-state interaction between the probe and protein.^{2, 20, 31} Thus fluorescence lifetime data can significantly contribute in realizing the interaction behavior between ellipticine and BSA. The typical time-resolved fluorescence decay profiles are displayed in **Figure S5** and the fitting parameters are summarized in **Table S1 and S2**. The decay profile of free drug (PBS, pH7) monitored at 525 nm (**Table S1**) is found to exhibit bi-exponential feature with the lifetime component of 2 ns (92%) and 5.38 ns (8%). In aqueous buffer ellipticine mainly exists in protonated form,^{10, 11, 13, 16} hence, we believe the dominant contribution (92%) of 2 ns component corresponds to the lifetime of protonated ellipticine; whereas 5.38 ns component is unlikely to appear from neutral ellipticine, as neutral form of the drug does not show any emission at 525 nm. However, tautomeric form of ellipticine can contribute towards the 525 nm emission intensity, although the quantum yield is very low in water. Therefore, we anticipate that 5.38 ns lifetime reflects the

lifetime of tautomeric form of ellipticine, which has minute population in water. In presence of protein, the contribution from the protonated form of ellipticine (~ 2 ns) decreases sharply, whereas a long component of ~ 16 ns to ~ 19 ns appears in place of 5.38 ns component (**Table S1**). The newly appeared long component is believed to be an outcome of protonated (or tautomeric) ellipticine bound to the protein binding pocket, and it corroborates well with the steady state results where we have observed that protonated ellipticine also participates in BSA

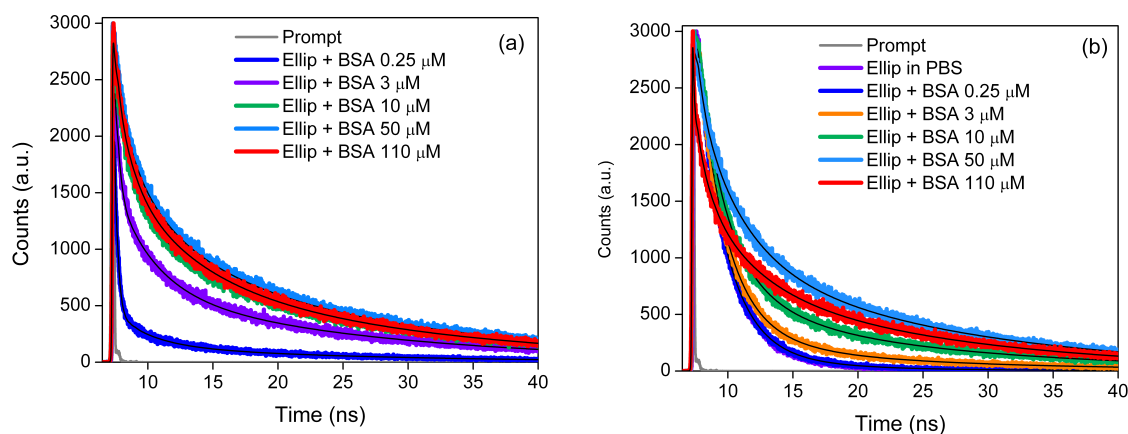


Figure S5: Lifetime decay profile of ellipticine in PBS and with increasing BSA concentrations collected at (a) 440 nm and (b) 525 nm, respectively.

binding. At higher protein concentration a fast component of ~ 500 ps appears in addition to other two components. We believe that due to the increased crowdedness at higher protein concentration, the drug molecules cannot easily access the binding pocket of protein. However, due to the Brownian motion as well as electrostatic attraction, drug molecules can easily repose on protein surface. The short lifetime might be outcome of the strong electrostatic attraction between the protonated ellipticine and negatively charged side chains of amino acid at the protein surface, by which electronic structure of protonated ellipticine is getting perturbed.

To get insight about the dynamics of neutral ellipticine generated in presence of protein, we have also collected lifetime at 440 nm (**Figure S5, Table S2**). At $0.25 \mu\text{M}$ of protein concentration, a tri-exponential decay shows lifetime components of 220 ps (90%), 2.67 ns (7%) and a long lifetime 17 ns (3%). It is reported that ellipticine in non-polar solvents (like dioxane,

cyclohexane, hexane etc.) exhibits very long lifetime,¹¹ and in these non-polar media ellipticine is likely to exist exclusively in neutral form due to the reduced pK_a of protonation in these non-polar environment.^{10, 11} Hence 17 ns lifetime is attributed to neutral ellipticine inside the protein nano-cavity, where it experiences a relatively high hydrophobicity. A glance at **Table S2** reveals that the contribution of this long component increases with rising BSA concentration, which proves that a dominant fraction of neutral ellipticine enters inside the protein binding pocket, and it is in well agreement with the steady state results where we have observed that the intensity of neutral ellipticine is progressively enhanced in presence of BSA. The appearance of ~2.5 ns component, which is matching with the lifetime of protonated ellipticine, is unusual as neutral ellipticine molecules exclusively contribute at 440 nm. Moreover, the contribution of this component increases as protein concentration increases. It is already observed from deconvoluted emission profiles that protonated form of ellipticine has significant intensity contribution even at 440 nm, and its contribution increases sharply, as the protein concentration increases. Hence, ~2.5 ns component appeared in the decay profile of 440 nm is attributed to the protonated ellipticine molecules those are free or unbound. The existence of relatively shorter lifetime (200-700 ps) in presence of protein environment is more interesting. At low BSA concentration the 220 ps component has a very high contribution of ~90%, and with increasing BSA concentration the component lifetime slightly increases but the contribution decreases sharply. We anticipate that the fastest component (~200-700 ps) reflects the dynamics of neutral ellipticine attached to the surface of protein by strong hydrogen bond with the side chains of amino acids. The reduced lifetime value can probably be attributed to energy dissipation via the vibrations associated with the intermolecular hydrogen bonding between N-H of the pyrrole ring and -OH/O⁻/-NH₂/-S/-SH group of amino acid side chains.¹³

(f) Time resolved anisotropy measurements:

We have also performed time resolved anisotropy measurement,^{2, 29, 32, 33} a sensitive tool, which will provide a notion about the rotational relaxation of the drug when it binds to the protein. The typical anisotropy decay profile of ellipticine in aqueous buffer as well as protein environment is shown in **Figure S6**. The drug exhibits a single exponential decay in aqueous buffer with rotational relaxation time of ~130 ps (**Table S3**). As in aqueous buffer ellipticine

exists mainly in protonated form, the anisotropy decay in water only provides idea about the rotational relaxation of protonated ellipticine molecules. However, we believe that if neutral ellipticine would have existed in water, would have shown similar relaxation time, as both forms differ only with respect to single proton. In presence of protein environment, anisotropy decay time for both neutral and protonated ellipticine slows down, implying protein induced confinement for both of the forms (**Figure S6**). Astonishingly, at lower concentration of protein (1 μM and 10 μM) a growth component is also observed which leads to unusual ‘dip-rise’ feature in the anisotropy decay (**Figure S6**). This kind of not-so-common time-resolved anisotropy arises due to the presence of multiple species, each characterized by its own lifetime and anisotropy decay.³⁴⁻³⁸ However, at higher protein concentration, the ‘dip-rise’ feature is absent, and the decay exhibits some residual anisotropy, which does not decay within our experimental time window. This is because at higher protein concentration, the population of short lifetime component reduces down significantly compared to long component population.

The detail fitting analysis of ‘dip-rise’ profile has been described here under. In case of “dip-rise” nature of anisotropy decay, we have to consider time dependence of weighing factor x_i , where x_i depends on the a_i , τ_i , and the total intensity decay, $I(t)$ by the following equation as suggested by Ludescher *et al.*³⁷

$$x_i(t) = \frac{a_i[\exp(-t/\tau_i)]}{I(t)} \quad (5)$$

Where, a_i is the percentage contribution of lifetime component τ_i , and $I(t)$ is the total decay. The final equation for dip rise anisotropy appears to be

$$r(t) = r_0 \frac{[\{R_1 \exp(-t/\tau_1) \times f_1 \exp(-t/\tau_{r1})\} + \{R_2 \exp(-t/\tau_2) \times f_2 \exp(-t/\tau_{r2})\}] + \{R_3 \exp(-t/\tau_3) \times f_2 \exp(-t/\tau_{r3})\}}{[R_1 \exp(-t/\tau_1) + R_2 \exp(-t/\tau_2) + R_3 \exp(-t/\tau_3)]} \quad (6)$$

where, r_0 known as residual anisotropy, τ_1 , τ_2 , τ_3 , are the lifetime components of the corresponding decays having a relative contribution of each component as R_1 , R_2 , and R_3 respectively. During ‘dip-rise’ anisotropy fit, the lifetime components and its relative contribution were kept fixed. The parameters obtained from fitting are presented in **Table S4**. For the sake of relevance of the present work, we are not going to discuss the detail about the ‘dip rise’ anisotropy feature.

The anisotropy decays of protonated ellipticine (collected at 530 nm) at higher protein concentrations are devoid of any ‘dip-rise’ features, and hence fitted by the following equation^{2, 29, 39}

$$r(t) = f_1 r_0 \exp\left(-\frac{t}{\tau_{r1}}\right) + f_2 r_0 \exp\left(-\frac{t}{\tau_{r2}}\right) + f_3 r_0 \exp\left(-\frac{t}{\tau_{r3}}\right) \quad (7)$$

where r_0 is the limiting anisotropy at $t = 0$, τ_{r1} reflects isotropic rotation of free drug in solution, τ_{r2} reflects slower reorientation time of drug bound to protein surface and τ_{r3} corresponds to the global tumbling motion of the protein bound drug molecule. f_1 , f_2 and f_3 are the relative contributions coming from τ_{r1} , τ_{r2} and τ_{r3} , respectively. It is found that anisotropy decays of

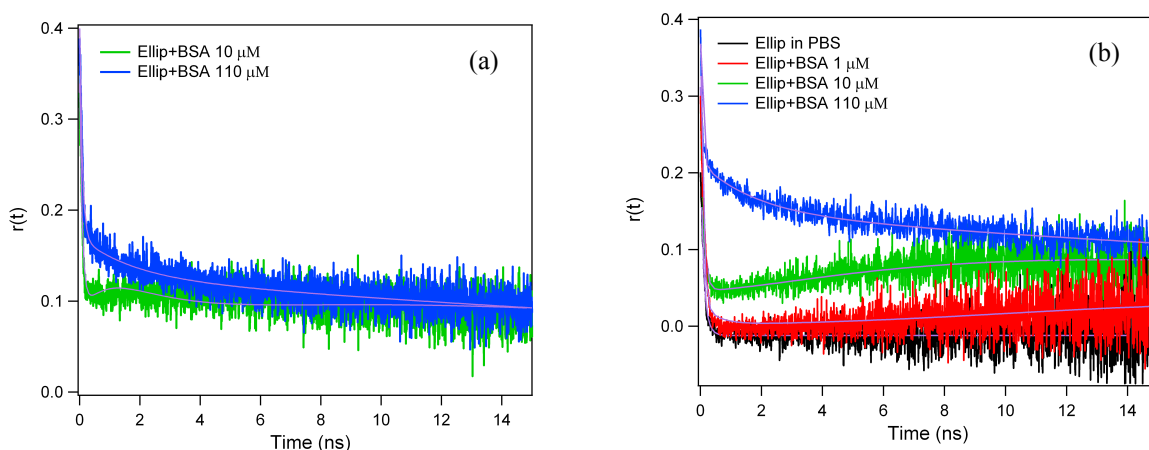


Figure S6: Anisotropy decay profile of ellipticine at various BSA concentrations collected at (a) 440 nm and (b) 525 nm, respectively.

protonated ellipticine (monitored at 525 nm) in presence of 110 μ M protein consists of three components, with a rotational relaxation times of ~ 130 ps, ~ 2 ns, and ~ 47 ns (**Table S3**). The

fast rotational relaxation component corresponds to the unbound ellipticine. Slower component might reflect either the segmental motion within the protein or surface bound protonated ellipticine, while the major contribution of the slowest component of ~ 47 ns is assigned as global tumbling of the protein. The anisotropy decay of neutral ellipticine monitored at 440 nm in presence of 110 μM protein concentration also consists of three components having similar rotational time constants as that of protonated one (**Table S3**). However, the percentage contribution of each component is slightly different. Here it is necessary to mention that protonated ellipticine also contributes to the anisotropy decay profile monitored at 440 nm, as it has some reasonable intensity at 440 nm. Therefore, the decay characteristics at 440 nm may not reflect the true anisotropy decay of neutral ellipticine. However, it provides conclusive evidence for the strong interaction between the neutral form of drug and protein.

Note 3: Circular Dichroism Spectra

The circular dichroism spectra of serum albumin (BSA) with increasing DNA concentration is shown here under (**Figure S5**). The results have been emphasized in detail to explain the protein DNA interaction in main manuscript.

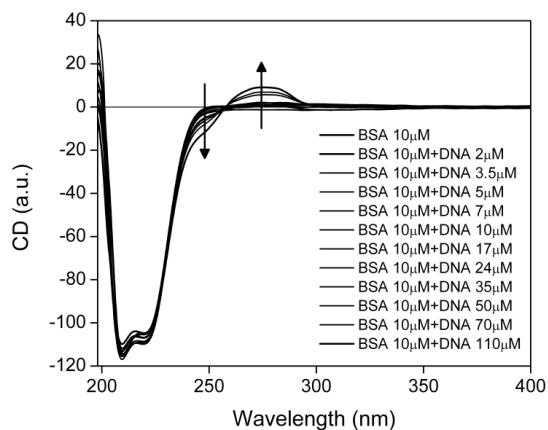


Figure S7: Circular dichroism spectra of BSA and DNA interaction. BSA (10 μM) is titrated with increasing DNA concentrations (legend carries the respective meaning).

Note 4: Ellipticine CT-DNA Interaction

Although the interaction behavior of ellipticine with DNA is well explored in the literature,^{10, 16, 40} in order to compare the interaction behavior with protein, we have probed the interaction characteristics between ellipticine and CT-DNA mainly through fluorescence measurements. A dramatic enhancement of the intensity at 525 nm peak, which is attributed to protonated ellipticine, is observed with the hike in DNA concentration (**Figure S8**). The huge enhancement of emission is an outcome of the intercalation of protonated ellipticine to DNA. Unlike protein environment, ellipticine does not bind to DNA in its neutral form, because of apparent increase of protonation pK_a due to the enhanced proton activity at the anionic interface.¹⁰ Intensity at peak maximum has been utilized to calculate the binding constant of ellipticine and DNA. The binding constant is estimated from Scatchard plot (**Note 2a**) determined to be $K=5.04 \times 10^5 \text{ M}^{-1}$, which is very close to the value obtained from chromatin bound ellipticine case.¹⁰ The higher binding affinity is also supported by steady state anisotropy measurement, where it is observed that with gradual addition of DNA anisotropy value of ellipticine rises up and gets saturated at $\sim 70 \mu\text{M}$ DNA (**Figure S8**). Above $70 \mu\text{M}$ the anisotropy value reaches to a plateau region (**Figure S8**), infers that the saturation in the binding interaction between the drug and DNA.

Fluorescence decay profiles of the drug in absence and presence of CT-DNA are shown in **Figure S8c** and the results are tabulated in **Table S1**. With the gradual addition of DNA, the percentage contribution of short lifetime component ($\sim 2 \text{ ns}$) progressively decreases, whereas a longer lifetime component of $\sim 12 \text{ ns}$ generates in the decay profile, and ultimately reaches to 96% at maximum DNA concentration. The increased lifetime of ellipticine in presence of DNA might be attributed to the enhanced stability of the drug by the stacking interaction with DNA. The interaction between ellipticine and DNA is also probed from time-resolved anisotropy measurements (**Figure S8**). Like protein, initial addition of DNA leads to ‘dip-rise’ feature of anisotropy decay profile. However, at higher DNA concentration the ‘dip-rise’ feature is totally vanished (**Figure S8**). Irrespective to anisotropy decay profiles, analysis clearly implies that the rotational relaxation of the drug is significantly retarded in presence of DNA (**Table S3 and S4**).

A very slow rotational relaxation time together with the existence of residual anisotropy reflects the intercalation is preferred binding mode of the drug to DNA.

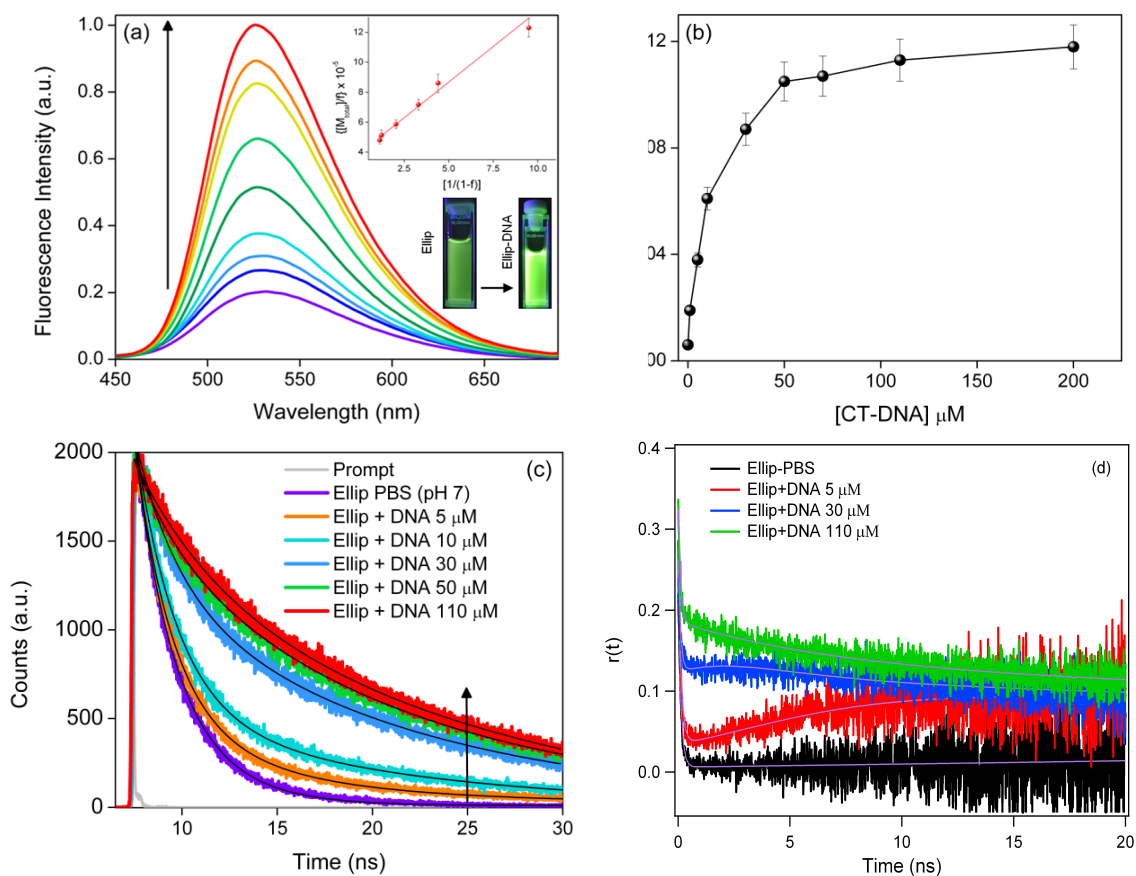


Figure S8: (a) Fluorescence emission spectra of ellipticine in PBS and with increasing DNA concentration ($[\text{DNA}] = 1, 5, 10, 20, 30, 50, 70, 110 \mu\text{M}$, respectively). Inset shows the Scatchard plot constructed from emission intensities. (b) Steady state anisotropy change of ellipticine at various DNA concentrations. (c) Lifetime decay profiles of ellipticine with various DNA concentrations. (d) Anisotropy decay profiles of ellipticine with various DNA concentrations.

Note 5: Protein-DNA Interaction

(a) Steady state emission spectra of ellipticine in HSA-DNA system:

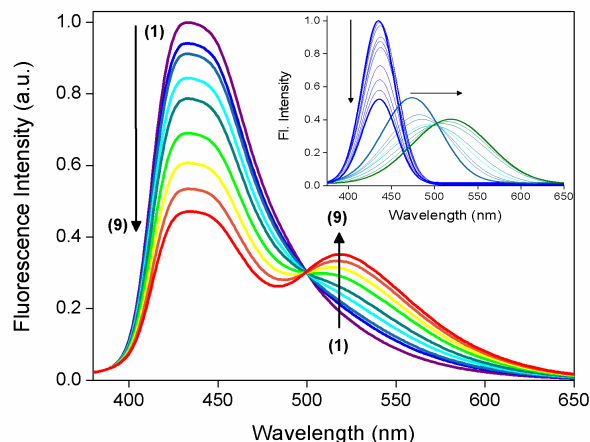


Figure S9: Fluorescence spectra of HSA-bound ellipticine with increasing concentration salmon sperm DNA, where the inset shows deconvoluted emission spectra for the same.

(b) Binding constant of protein-ellipticine-DNA ternary complex from Scatchard plot:

The binding constant of ellipticine-protein-DNA ternary complex (**Figure S10**) has been calculated from steady state emission spectra using modified Scatchard plot as described earlier (**Note 2a**).

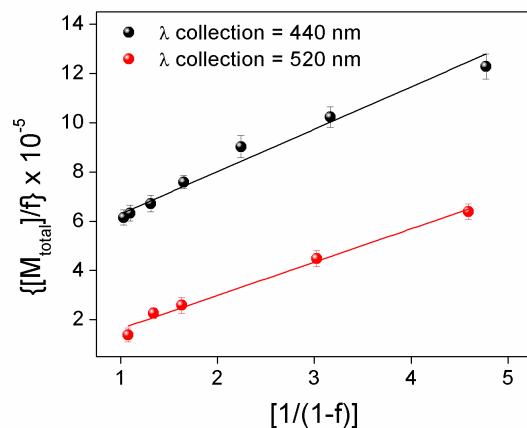


Figure S10: Binding constant determination at 440 nm and 520 nm using deconvoluted emission plot from modified Scatchard plot.

(c) Fluorescence lifetime measurements:

We have monitored the fluorescence lifetime of protein bound ellipticine with a raising concentration of DNA to get insight about the protein-DNA interaction scenario. The typical time-resolved decay profiles are depicted in **Figure S11** and the results are summarized in **Table S1 and S2**. The drug molecules show a multi-exponential decay profile, which is obvious for the case of micro-heterogeneous environment comprising both protein and DNA, and in such a case, it appears to be difficult to assign individual decay components. Therefore, it is rational to consider the average fluorescence lifetimes of the drug instead of emphasizing on individual decay components. It is noticeable from the results shown in **Table S2** that the average lifetime of BSA bound protonated drug (~ 7 ns) progressively increases with the gradual addition of DNA, and this is certainly an outcome of the interaction between protein bound drug and DNA. Steady state results have already provided a notion that protonated form of drug molecule involves in ternary complex formation. We believe that the increase in average lifetime of drug

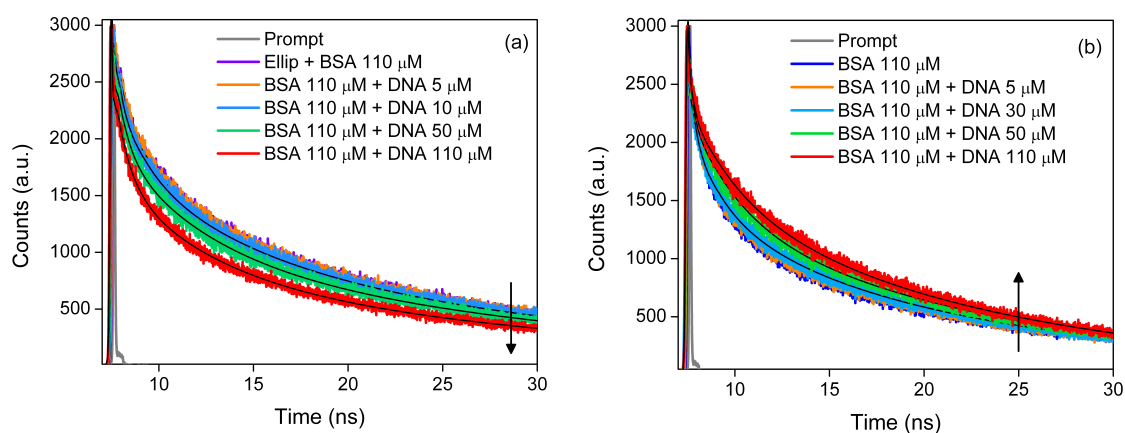


Figure S11: Lifetime decay profile of ellipticine-BSA with increasing DNA concentrations (shown in legend) collected at (a) 440 nm and (b) 525 nm respectively.

from 6-9 ns is an outcome of the same. Therefore, lifetime results pave a way for assessing the existence of ternary complex comprising of protein, DNA and protonated ellipticine. The average fluorescence lifetime of protein bound neutral ellipticine monitored at 440 nm progressively decreases with increasing DNA concentration, indicating the expulsion of neutral

ellipticine from its stronger binding sites to the proximity of bulk water. Hence, lifetime results corroborate the steady state results, where we have also noticed that the quantum yield of neutral ellipticine progressively decreases with the increasing DNA concentration.

(d) Time resolved anisotropy results:

We have further exploited fluorescence anisotropy technique to establish the interaction behaviour of ellipticine in presence of both protein and DNA. **Figure S12** depicts the typical anisotropy decays of protonated ellipticine (monitored at 525 nm) containing 110 μM of protein with increasing DNA concentration and the results are tabulated in **Table S3** as a function of DNA concentration. Anisotropy decay of protonated ellipticine in 110 μM protein concentration consists of three components, which are ~ 130 ps, ~ 2 ns, and a long component of 47 ns. The fast rotational relaxation component corresponds to the unbound ellipticine. Slower component might reflect either the segmental motion of the protein or the surface bound protonated ellipticine, while the major contribution of the slowest component of ~ 47 ns is assigned as global tumbling motion of the protein. With varying concentration of DNA, the time constant for long component increases, indicating retarded global tumbling motion due to the interaction with DNA (**Figure S12, Table S3**). The slowing down of global tumbling time-scale in presence of DNA actually

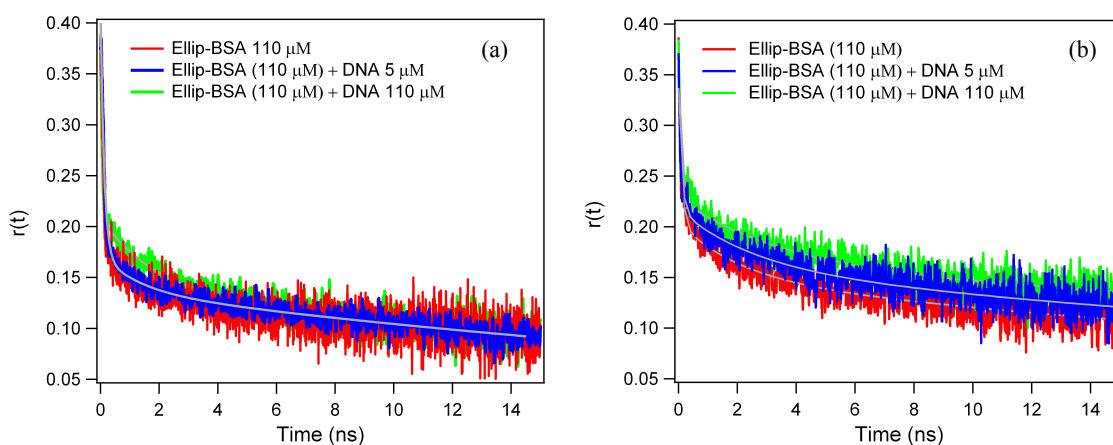


Figure S12: (a) Anisotropy decay profile of ellipticine-BSA at various DNA concentrations (shown in legend) collected at 440 nm and (b) 525 nm respectively.

actually supports the existence of ternary complex, by which the net hydrodynamic radius of the BSA-DNA complex increases and rotational relaxation becomes sluggish. Moreover, as the increment is not abruptly high, it is logical to anticipate that only a segment of DNA is involved in the ternary complex formation. It is already revealed from FTIR studies that CT-DNA interacts with serum albumin either through G-C rich region or through the phosphate backbone interaction of DNA.⁴¹ If the whole DNA was involved in the ternary complex formation, then it would have shown highly sluggish global tumbling motion along with a higher value of residual anisotropy.

Hydrodynamic volume of a molecule can be calculated using the time-scale of rotational diffusion. When a fluorophore diffuses through a solution with a rotational diffusion coefficient D_r the time resolved anisotropy of the probe can be expressed as:

$$r(t) = r_0 \exp(-6D_r t) \quad (8)$$

Whereas the basic equation for time resolves anisotropy is

$$r(t) = r_0 \exp\left(-\frac{t}{\tau_r}\right) \quad (9)$$

Comparing equation 8 and 9, τ_r is related to the diffusion coefficient as $\tau_r = (1/6D_r)$. Combining Stokes-Einstein⁴² along with relation of τ_r one can determine the hydrodynamic radius and hence hydrodynamic volume of a diffusing molecule with the help of following two equations.

$$D_r = \frac{1}{6\tau_r} = \frac{RT}{6v\eta} \quad (10)$$

$$v = \frac{4\pi\pi^3}{3} = \frac{RT\tau_r}{\eta} \quad (11)$$

Table S1: Lifetime results of ellipticine in buffer, BSA, CT-DNA and BSA-DNA systems collected at 525 nm.

Sample	τ_1 (ns)	τ_2 (ns)	τ_3 (ns)	R_1	R_2	R_3	$\tau_{av}^{\#}$	χ^2
(a)								
Ellip in PBS (pH 7)		2	5.38		0.92	0.08	2.31	1.00
Ellip + BSA 3 μ M		2.24	15.0		0.91	0.09	3.35	1.01
Ellip + BSA 10 μ M		2.30	16.0		0.57	0.43	8.15	1.00
Ellip + BSA 50 μ M	0.464	3.09	17.0	0.25	0.42	0.33	7.01	0.96
Ellip + BSA 110 μ M	0.510	2.89	16.7	0.32	0.29	0.39	7.50	0.99
(b)								
Ellip + DNA 5 μ M		2.06	11.70		0.49	0.51	3.54	1.05
Ellip + DNA 10 μ M		2.05	12.75		0.32	0.68	4.75	1.03
Ellip + DNA 50 μ M		2.00	13.8		0.06	0.94	10.6	1.03
Ellip + DNA 110 μ M		2.82	14.43		0.04	0.96	12.32	1.02
(c)								
Ellip-BSA + DNA 5 μ M	0.530	3.00	16.34	0.32	0.28	0.41	7.73	1.02
Ellip-BSA + DNA 30 μ M	0.535	3.10	16.13	0.28	0.28	0.44	8.10	1.01
Ellip-BSA + DNA 50 μ M	0.610	3.40	15.60	0.29	0.24	0.47	8.40	1.02
Ellip-BSA + DNA 100 μ M	0.535	3.13	15.00	0.23	0.23	0.54	8.96	1.01

$$\tau_{av}^{\#} = \tau_1 R_1 + \tau_2 R_2 + \tau_3 R_3$$

Table S2: Lifetime results of ellipticine with BSA and BSA-bound ellipticine titrated by increasing CT-DNA concentrations (collection wavelength=440 nm).

Sample	τ_1 (ns)	τ_2 (ns)	τ_3 (ns)	R_1	R_2	R_3	$\tau_{av}^{\#}$	χ^2
(a)								
Ellip + BSA 0.25 μ M	0.220	2.67	17.00	0.90	0.07	0.03	0.900	1.02
Ellip + BSA 3 μ M	0.273	2.80	17.82	0.58	0.24	0.18	3.98	1.03
Ellip + BSA 10 μ M	0.501	3.31	18.47	0.42	0.31	0.27	6.35	0.98
Ellip + BSA 50 μ M	0.717	4.08	19.05	0.38	0.30	0.32	7.58	1.06
Ellip + BSA 110 μ M	0.661	4.53	19.40	0.41	0.31	0.27	6.96	1.02
(b)								
Ellip-BSA + DNA 5 μ M	0.461	4.15	21.16	0.36	0.26	0.36	8.97	1.01
Ellip-BSA + DNA 10 μ M	0.454	3.94	21.40	0.38	0.26	0.35	8.77	1.03
Ellip-BSA + DNA 50 μ M	0.221	3.30	20.72	0.46	0.25	0.29	6.91	1.10
Ellip-BSA + DNA 100 μ M	0.176	2.88	20.22	0.54	0.23	0.23	5.42	1.06

$$\tau_{av}^{\#} = \tau_1 R_1 + \tau_2 R_2 + \tau_3 R_3$$

Table S3: Anisotropy fitting results (equation 7) of ellipticine in buffer, BSA, DNA and BSA-DNA systems.

Sample	τ_{r1} (ns)	τ_{r2} (ns)	τ_{r3} (ns)	f_1	f_2	f_3	r_0
(a)							
Ellip in PBS 525 nm	0.13	-	-	0.39	-	-	0.39
Ellip + BSA (110 μ M) at 440 nm	0.08	1.86	45	0.23	0.04	0.12	0.39
Ellip + BSA (110 μ M) at 525 nm	0.13	2.0	47	0.18	0.06	0.15	0.39
(b)							
Ellip + DNA (50 μ M) at 525 nm	0.09	6.82	100	0.24	0.03	0.13	0.40
Ellip + DNA (70 μ M) at 525 nm	0.09	5.82	110	0.17	0.05	0.14	0.36
Ellip + DNA (110 μ M) at 525 nm	0.09	4.87	93	0.14	0.05	0.14	0.33
(c)							
Ellip-BSA + DNA 5 μ M (440 nm)	0.12	1.83	50	0.21	0.05	0.13	0.39
Ellip-BSA + DNA 30 μ M (440 nm)	0.12	2.48	50	0.19	0.04	0.13	0.36
Ellip-BSA + DNA 30 μ M (440 nm)	0.12	2.93	48	0.14	0.07	0.13	0.34
Ellip-BSA + DNA 5 μ M (525 nm)	0.10	2.64	54	0.12	0.06	0.16	0.34
Ellip-BSA + DNA 30 μ M (525 nm)	0.10	3.08	60	0.12	0.08	0.14	0.34
Ellip-BSA + DNA 30 μ M (525 nm)	0.10	3.50	83	0.14	0.07	0.16	0.37

Table S4: Fitting parameters of ‘dip-rise’ anisotropy decay features of ellipticine-BSA and ellipticine-DNA systems.

Sample	τ_{r1} (ns)	τ_{r2} (ns)	τ_{r3} (ns)	a_1	a_2	a_3	r_0
(a)							
Ellip + BSA (1 μ M) at 440 nm	0.075	1.32	37.34	0.92	1.36	0.31	0.40
Ellip + BSA (10 μ M) at 440 nm	0.091	3	45	2.08	0.40	0.50	0.27
Ellip + BSA (1 μ M) at 525 nm	0.08	1	48	2.0	0.13	0.15	0.30
Ellip + BSA (10 μ M) at 525 nm	0.1	2.38	45	1.61	0.32	0.45	0.30
(b)							
Ellip + DNA (5 μ M) at 525 nm	0.1	5	100	2.09	0.24	0.47	0.25
Ellip + DNA (30 μ M) at 525 nm	0.1	8.0	100	1.45	1.74	0.44	0.27

Reference

1. A. Sengupta and P. Hazra, *Chem. Phys. Lett.*, 2010, **501**, 33-38.
2. A. Sengupta, W. D. Sasikala, A. Mukherjee and P. Hazra, *ChemPhysChem*, 2012, **13**, 2142-2153.
3. K. Gavvala, W. D. Sasikala, A. Sengupta, S. A. Dalvi, A. Mukherjee and P. Hazra, *Phys.Chem.Chem.Phys.*, 2013, **15**, 330-340.
4. K. Gavvala, A. Sengupta and P. Hazra, *ChemPhysChem*, 2013, **14**, 532-542.
5. <http://www.rcsb.org/pdb/explore/explore.do?structureId=3V03>,
<http://www.rcsb.org/pdb/explore/explore.do?structureId=3V03>.
6. G. M. Morris, R. Huey, W. Lindstrom, M. F. Sanner, R. K. Belew, D. S. Goodsell and A. J. Olson, *J. Comput. Chem.*, 2009, **30**, 2785-2791.
7. C. Hetényi and D. van der Spoel, *FEBS Lett.*, 2006, **580**, 1447-1450.
8. G. M. Morris, D. S. Goodsell, R. S. Halliday, R. Huey, W. E. Hart, R. K. Belew and A. J. Olson, *J. Comput. Chem.*, 1998, **19**, 1639-1662.
9. E. F. Pettersen, T. D. Goddard, C. C. Huang, G. S. Couch, D. M. Greenblatt, E. C. Meng and T. E. Ferrin, *J. Comput. Chem.*, 2004, **25**, 1605-1612.
10. F. Sureau, F. Moreau, J. M. Millot, M. Manfait, B. Allard, J. Aubard and M. A. Schwaller, *Biophys. J.*, 1993, **65**, 1767-1774.
11. S. Y. Fung, J. Duhamel and P. Chen, *J. Phys. Chem. A*, 2006, **110**, 11446-11454.
12. S. Banerjee, A. Pabbathi, M. C. Sekhar and A. Samanta, *The Journal of Physical Chemistry A*, 2011, **115**, 9217-9225.
13. Z. Miskolczy, L. Biczók and I. Jablonkai, *Chem. Phys. Lett.*, 2006, **427**, 76-81.
14. R. Thakur, A. Das and A. Chakraborty, *J.Photochem. Photobiol. B: Biology*, DOI: <http://dx.doi.org/10.1016/j.jphotobiol.2013.10.016>.
15. D. V. Matyushov, R. Schmid and B. M. Ladanyi, *J. Phys. Chem. B*, 1997, **101**, 1035-1050.
16. S. J. Froelich-Ammon, M. W. Patchan, N. Osheroff and R. B. Thompson, *J. Biol. Chem.*, 1995, **270**, 14998-15004.
17. O. Sedlacek, M. Hruby, M. Studenovsky, J. Kucka, D. Vetvicka, L. Kovar, B. Rihova and K. Ulbrich, *Bioconjugate Chem.*, 2011, **22**, 1194-1201.
18. E. F. Healy, *J. Chem. Educ.*, 2007, **84**, 1304.
19. T. P. Silverstein, *J. Chem. Educ.*, 2008, **85**, 1192.
20. B. K. Paul and N. Guchhait, *J. Phys. Chem. B: Biology*, 2011, **115**, 10322-10334. DOI: <http://dx.doi.org/10.1016/j.jphotobiol.2013.10.016>
21. A. Bolli, M. Marino, G. Rimbach, G. Fanali, M. Fasano and P. Ascenzi, *Biochem. Biophys. Res. Commun.*, 2010, **398**, 444-449.
22. Z. Chi, R. Liu, Y. Teng, X. Fang and C. Gao, *J. Agric. Food. Chem.*, 2010, **58**, 10262-10269.
23. A. Chakrabarty, A. Mallick, B. Haldar, P. Das and N. Chattopadhyay, *Biomacromolecules*, 2007, **8**, 920-927.
24. M. Bruchez, M. Moronne, P. Gin, S. Weiss and A. P. Alivisatos, *Science*, 1998, **281**, 2013-2016.
25. W. C. W. Chan and S. Nie, *Science*, 1998, **281**, 2016-2018.
26. X. M. He and D. C. Carter, *Nature*, 1992, **358**, 209.
27. T. Peters Jr, in *Adv. Protein Chem.*, eds. J. T. E. C.B. Anfinsen and M. R. Frederic, Academic Press, 1985, vol. Volume 37, pp. 161-245.
28. B. K. Paul, A. Samanta and N. Guchhait, *J. Phys. Chem. B*, 2010, **114**, 6183-6196.

29. J. R. Lakowicz, *Principles of Fluorescence Spectroscopy*, Springer Science, New York, USA, 2006.
30. S. Ghosh, S. Jana and N. Guchhait, *J. Phys. Chem. B*, 2011, **116**, 1155-1163.
31. A. Sengupta, R. V. Khade and P. Hazra, *J. Photochem. Photobiol. A: Chemistry*, 2011, **221**, 105-112.
32. E. Deprez, P. Tauc, H. Leh, J.-F. Mouscadet, C. Auclair, M. E. Hawkins and J.-C. Brochon, *Proc. Natl. Acad. Sci. U.S.A.*, 2001, **98**, 10090-10095.
33. K.-S. Chang, L. Luo, C.-W. Chang, Y.-C. Huang, C.-Y. Cheng, C.-S. Hung, E. W.-G. Diao and Y.-K. Li, *J. Phys. Chem. B*, 2010, **114**, 4327-4334.
34. S. S. Sinha, R. K. Mitra and S. K. Pal, *J. Phys. Chem. B*, 2008, **112**, 4884-4891.
35. C. R. Guest, R. A. Hochstrasser, D. J. Allen, S. J. Benkovic, D. P. Millar and C. G. Dupuy, *Biochemistry*, 1991, **30**, 8759-8770.
36. T. Kanti Das and S. Mazumdar, *Biophys. Chem.*, 2000, **86**, 15-28.
37. R. D. Ludescher, L. Peting, S. Hudson and B. Hudson, *Biophys. Chem.*, 1987, **28**, 59-75.
38. B. Bhattacharya, S. Nakka, L. Guruprasad and A. Samanta, *J. Phys. Chem. B*, 2009, **113**, 2143-2150.
39. T. Goel, T. Mukherjee, B. J. Rao and G. Krishnamoorthy, *J. Phys. Chem. B*, 2010, **114**, 8986-8993.
40. A. Das, R. Thakur and A. Chakraborty, *RSC Advances*, 2013, **3**, 19572-19581.
41. H. Malonga, J. F. Neault, H. Arakawa and H. A. Tajmir-Riahi, *DNA and Cell Biol.*, 2006, **25**, 63-68.
42. G. R. Fleming, *Oxford university press, NY*, 1986.